Control Engineering Practice 17 (2009) 1432–1439

Contents lists available at ScienceDirect

Control Engineering Practice

journal homepage: www.elsevier.com/locate/conengprac

Motion planning for experimental air path control of a variable-valve-timing spark ignition engine

Thomas Leroy [a,b,*], Jonathan Chauvin [a], Nicolas Petit [b]

[a] Institut Français du Pétrole, 1 et 4 Avenue de Bois Préau, 92852 Rueil-Malmaison, France
[b] Centre Automatique et Systèmes, Mathématiques et Systémes, Mines-ParisTech 60, bd St Michel, 75272 Paris, France

ARTICLE INFO

Article history:
Received 15 May 2008
Accepted 13 October 2008
Available online 1 December 2008

Keywords:
Engine control
Spark ignition engines
Time-varying systems
Nonlinear observers

ABSTRACT

Air path control of a spark ignition engine without an EGR loop, equipped with variable-valve-timing (VVT) actuators, is addressed in this paper. VVT devices are used to produce internal exhaust gas recirculation, providing beneficial effects in terms of fuel consumption and pollutant emissions reduction. However, VVT actuators affect the fresh air charge in the cylinders. This has an impact on the torque output (leading to driveability problems) and on the fuel/air ratio (FAR) (leading to pollution peaks). To compensate for these undesirable effects, a new approach is proposed. Supportive experimental results show the relevance of this approach.

1. Introduction

1.1. Motivation

Lately, variable-valve-timing (VVT) actuators have been used in spark ignition (SI) engines to exploit all of the possibilities of direct injection and turbocharging. This approach is of particular interest in the context of downsizing (reduction of the engine size), which has appeared as a major solution to the problem of reducing fuel consumption (see Lecointe & Monnier, 2003). In the present study, the engine under consideration was not equipped with any exhaust gas recirculation (EGR) capability.

VVT systems use electrohydraulic mechanisms which rotate the camshaft to modify the breathing of the engine. A beneficial effect is a reduction of the pumping losses. For a given engine torque output, an increase in the valve overlap (the number of crankshaft angle degrees during which both valves are opened) implies an increase in the intake manifold pressure (see Fig. 1a). The negative work necessary to suck air into the cylinder is then reduced. VVT systems also allow internal EGR, leading to reduction in emissions of nitrogen oxides (NO_x) (Shaver, Roelle, & Christian Gerdes, 2006) (see Fig. 1b).

1.2. Control problem

One basic task in engine control is managing the torque output of the engine according to the driver's requirements, while limiting pollutant emissions. Torque control is achieved by managing the in-cylinder air mass, while keeping the fuel/air ratio (FAR) to the stoichiometric value in order to maximize the efficiency of the three-way catalyst and thus minimize the pollutants (CO, hydrocarbons, and NO_x) created by combustion (Guzzella & Onder, 2004).

In conventional SI engines, a reference in-cylinder air mass is computed directly from the intake manifold pressure through a quasi-static relation depending on the volumetric efficiency (see Heywood, 1988). Controlling the air is achieved by modulation of the intake pressure through the intake throttle (see Khiar et al., 2007 for example). In parallel, the FAR management consists classically of a PID controller using a FAR measurement (given by an oxygen sensor situated at the engine exhaust), which is complemented by a feedforward control law to limit FAR fluctuations during torque transients (Grizzle, Cook, & Milam, 1994). The FAR controller acts upon the reference fuel mass which is sent to the injection system. The feedforward control law is designed according to a prediction of the air mass in the cylinders (Chevalier, Vigild, & Hendricks, 2000).

In SI engines equipped with VVT actuators, the in-cylinder air mass depends also on the positions of the VVT actuators. Thus, VVT has an impact on the volumetric efficiency of the aspiration from the intake manifold into the cylinders (see Heywood, 1988). Its influence can be modeled (see Colin, Chamaillard, Bloch, & Corde, 2007; Leroy, Chauvin, Le Berr, Duparchy, & Alix, 2008;

* Corresponding author at: Institut Français du Pétrole, 1 et 4 Avenue de Bois Préau, 92852 Rueil-Malmaison, France. Tel.: +33 1 47 52 81 91; fax: +33 1 47 52 70 12.
E-mail address: thomas.leroy@ifp.fr (T. Leroy).

0967-0661/$ - see front matter © 2008 Elsevier Ltd. All rights reserved.
doi:10.1016/j.conengprac.2008.10.010

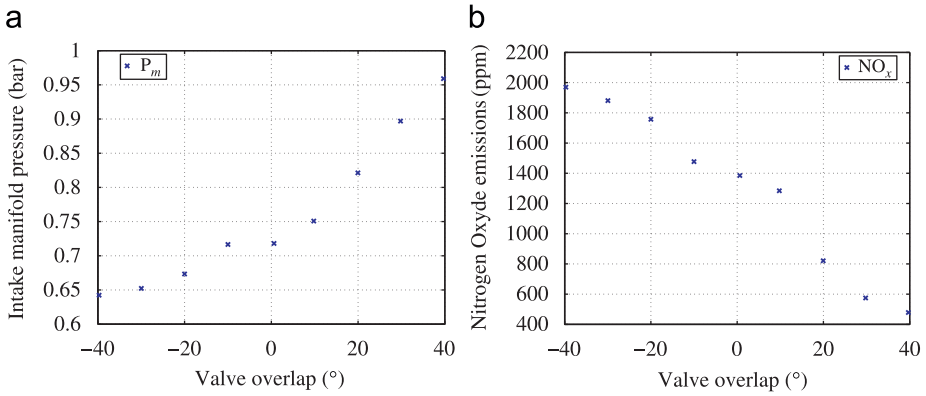

Fig. 1. Experimental (a) intake manifold pressure and (b) NO_x measurements as a function of the valve overlap at constant indicated mean effective pressure (5 bar) and constant engine speed (2000 rpm).

Stefanopoulou, Cook, Grizzle, & Freudenberg, 1998, for example), but errors cannot be avoided, leading to in-cylinder prediction errors, which unavoidably propagate, through feedforward terms, into the FAR management system. This issue generates pollution peaks and results in poor driveability.

1.3. Proposed control strategy

A simple alternative solution is proposed here. Focusing on the in-cylinder air mass control problem only, two types of modeling errors are compensated with an improved control strategy. The intake dynamics is modeled as a first-order system, using the above-mentioned volumetric efficiency related to the VVT actuators, and one consider two biases. One of these represents errors in the experimentally determined look-up table of the throttle effective area. The other accounts for errors in the volumetric-efficiency law. Provided that these biases are known, one obtains a one-dimensional actuated dynamics, for which the motion-planning and trajectory-tracking problems are already solved. From a more realistic standpoint, a compensation of these two biases can be obtained by use of an integral term and an observer. In parallel, the FAR management system simply assumes that the reference signal for the in-cylinder air mass is tracked. Experimental results prove the relevance of this approach.

This paper is organized as follows. In Section 2, the reference model for the intake manifold is presented. This model consists of mass balance and aspirated-flow equations. The control problem is also presented in this section. In Section 3, the control strategy is outlined. The first part considers generation of the motion-planning trajectory of the intake manifold pressure from a torque set point. Then, feedforward and feedback control laws are presented. In Section 4, experimental results obtained on a test bench are shown.

2. Control problem and system modeling

2.1. Air path modeling

In numerous references found in the literature (e.g. Chevalier, Müller, & Hendricks, 2000), mean-value engine modeling approaches are presented as a reliable and efficient way to represent engine dynamics. Because the complexity of the model impacts on the design of the control system, however, a simplified model of the intake manifold is proposed here.

2.1.1. Balance in the intake manifold

Notation is provided after Conclusions. Consider the air path of an SI engine equipped with VVT actuators as depicted in Fig. 2. In this configuration, i.e. with internal EGR, the air path has a very simple structure. It can be modeled by an intake manifold which has an inlet flow (controlled by the throttle) and an outlet flow (impacted on by the VVT actuators). The intake manifold is considered to have a constant volume, in which the thermodynamic state (pressure, temperature, and composition) is assumed to be spatially homogeneous. Also, time variations of the temperature are neglected in this volume (following Andersson & Eriksson, 2001; Guzzella & Onder, 2004), i.e. $\dot{T}_m = 0$. Under these assumptions, a mass balance in the intake manifold gives

$$\dot{P}_m = \alpha_m(\dot{m}_{at} - \dot{m}_{asp}) \tag{1}$$

where $\alpha_m \triangleq RT_m/V_m$. Both P_m and T_m are measured by sensors located in the intake manifold. $\dot{m}_{at}$ is the intake mass air flow. In this study, one neglect the intercooler volume. Then, $\dot{m}_{at}$ can be well approximated by the mass air flow measured at the intake, $\dot{m}_{MAF}$. Correspondingly, $\dot{m}_{asp}$ is the mass air flow aspirated into the cylinders.

The intake mass air flow, $\dot{m}_{at}$, can be modeled in the form

$$\dot{m}_{at} = Area_{th} \cdot f(P_m) \tag{2}$$

where $Area_{th}$ is the effective opening area of the throttle. The mass flow rate per unit area, $f(P_m)$, is given in Heywood (1988), in the form

$$f(P_m) = \frac{P_{dc}}{\sqrt{RT_m}} \begin{cases} \left(\frac{P_m}{P_{dc}}\right)^{1/\gamma} \sqrt{\frac{2\gamma}{\gamma-1}\left(1-\left(\frac{P_m}{P_{dc}}\right)^{(\gamma-1)/\gamma}\right)} & \text{if } \left(\frac{P_m}{P_{dc}}\right) > 0.528 \\ \sqrt{\gamma\left(\frac{2}{\gamma+1}\right)^{(\gamma+1)/(\gamma-1)}} & \text{otherwise} \end{cases} \tag{3}$$

where P_{dc} is the measured downstream compressor pressure, and γ is the ratio of specific heat capacities in the intake manifold.

The effective area of the throttle is usually modeled with a polynomial function of the angular position of the actuator, i.e. $Area_{th} = \mathscr{A}(\theta_{th})$. Fig. 3 presents the modeled and experimental opening areas of the throttle as a function of the angular position of the actuator.

As the model (2) is not perfect, one can add a modeling error term ε_{th}, leading to the following relation:

$$\dot{m}_{at} = \mathscr{A}(\theta_{th})f(P_m) + \varepsilon_{th} \tag{4}$$

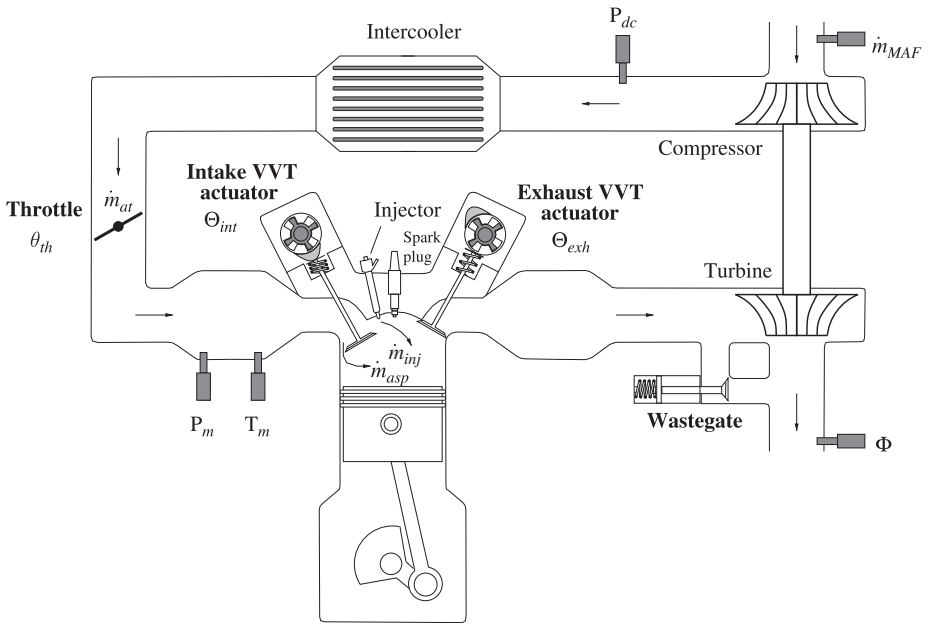

Fig. 2. Air path scheme. The intake mass air flow ($\dot{m}_{MAF}$), downstream compressor pressure (P_{dc}), intake manifold pressure and temperature (P_m and T_m), and fuel/air ratio (Φ) are measured by sensors; $\dot{m}_{at}$ is the throttle mass air flow and $\dot{m}_{asp}$ is the unknown aspirated mass air flow; θ_{th}, Θ_{int}, and Θ_{exh} are the angular positions of the actuators.

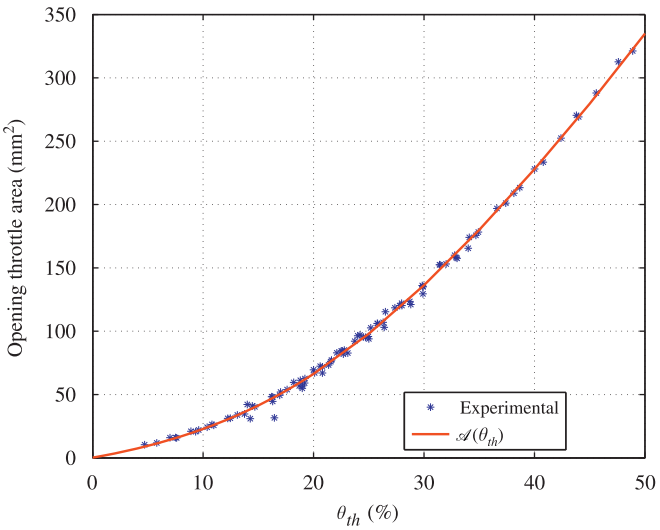

Fig. 3. Modeling error in the throttle opening area.

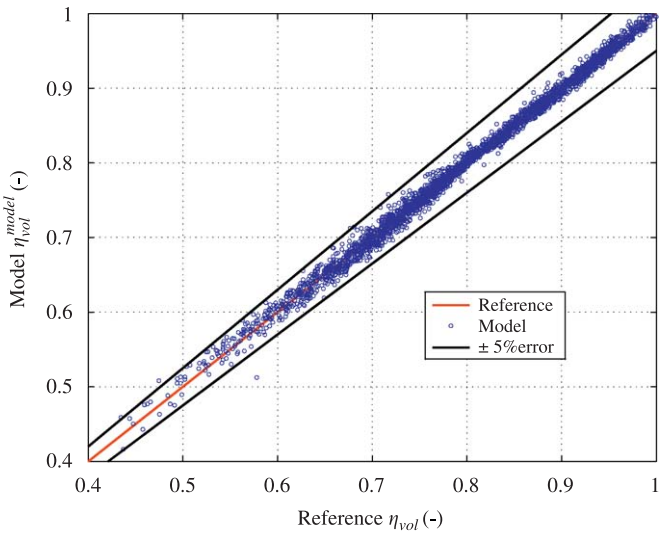

Fig. 4. Comparison between modeled and experimental volumetric efficiencies, η_{vol}^{model} and η_{vol}.

Following Heywood (1988), the mass air flow through the inlet valves is modeled in the form

$$\dot{m}_{asp} = \eta_{vol}\beta_m P_m \tag{5}$$

where $\beta_m \triangleq (V_d/RT_m)(N_e/120)$ and η_{vol} is the volumetric efficiency. In fixed-valve-timing engines, η_{vol} is a look-up table function of the intake manifold pressure and engine speed. In VVT engines, this simple relation can no longer be used, since VVT actuators drastically affect the in-cylinder air mass. A model using the positions of the VVT actuators has been presented by Leroy, Chauvin, Le Berr et al. (2008). This models the aspirated air mass in the cylinder using geometrical engine parameters, and gives

$$m_{asp}^{model} = \alpha_1 \frac{P_m V_{ivc}(\Theta_{int})}{RT_m} - \alpha_2 \frac{\mathrm{OF}(\Theta_{int}, \Theta_{exh})}{N_e} - \alpha_3 V_{evc}(\Theta_{exh}) \tag{6}$$

where α_1, α_2, and α_3 are look-up table functions of the intake manifold pressure and engine speed. V_{ivc} defines the in-cylinder volume at intake valve closing (a function of the intake VVT), V_{evc} defines the in-cylinder volume at exhaust valve closing (a function of the exhaust VVT), and OF defines the overlap factor (a function of both VVTs). Then, using (6), one can derive a model of the volumetric efficiency

$$\eta_{vol}^{model} = m_{asp}^{model} \frac{P_m V_d}{RT_m}$$

Fig. 4 shows a comparison between the experimental and modeled volumetric efficiency over a large range of operating conditions (engine speed from 750 to 3000 rpm, intake manifold pressure from 0.3 to 2 bar, and all VVT actuator positions).

Let $\eta_{\Delta}(P_m) = \eta_{vol}^{model}$ with $\Delta \triangleq (N_e, \Theta_{int}, \Theta_{exh}) \in \mathbb{R}^3$. Considering model uncertainties, one can add a bias $\delta\eta$ to compensate for modeling errors. Then, (5) becomes

$$\dot{m}_{asp} = (\eta_{\Delta}(P_m) + \delta\eta)\beta_m P_m \tag{7}$$

The bias $\delta\eta$ is completely unknown when it represents the modeling error in the volumetric efficiency. Following ideas of Andersson and Eriksson (2001) and Stotsky and Kolmanovsky (2002), one assume a constant bias, i.e. $\dot{\delta\eta} = 0$.

2.1.2. State space model

One uses $x \triangleq [P_m \;\; \delta\eta \;\; \varepsilon_{th}]^T$ and $u \triangleq \theta_{th}$ to denote the state and the control variable of the system, respectively. The measurements are $y_1 \triangleq x_1$ and $y_2 \triangleq \dot{m}_{MAF}$. Gathering (1), (4), and (7) together, one can write

$$\begin{cases} \dot{x}_1 = \alpha_m(\mathscr{A}(u)f(x_1) + x_3 - (\eta_{\Delta}(x_1) + x_2)\beta_m x_1) \\ \dot{x}_2 = 0 \\ \dot{x}_3 = 0 \\ y_1 = x_1 \\ y_2 = \mathscr{A}(u)f(x_1) + x_3 \end{cases} \tag{8}$$

2.2. Control problem

The goal is to control the air mass aspirated into the cylinders. Three actuators have an influence on this variable: the throttle, the intake VVT actuator, and the exhaust VVT actuator (see Fig. 2).

VVT actuators possess undebatable advantages in terms of combustion efficiency. However, analysis of the internal EGR shows that it has some interaction with the slow filling dynamics of the intake manifold, which can cause unacceptable engine performance (Stefanopoulou & Kolmanovsky, 1999). Many authors have proposed transient control strategies to compensate for the side effects of VVT actuators. In Stefanopoulou & Kolmanovsky (1997), a dynamic camshaft scheduling scheme based on the throttle position and engine speed, to obtain a torque response similar to that of a fixed-valve-timing engine, is presented. Another point of view can be considered. In Jankovic, Frischmuth, Stefanopoulou, and Cook (1998) and Jankovic (2002), VVT actuators are seen as a disturbance to the in-cylinder air mass control. This disturbance is taken into account in the throttle control strategy.

In the study presented here, control of the air mass through the throttle is achieved by taking into account VVT variations which are considered as measured disturbances. Since the throttle permits one to control the intake manifold pressure, one can turn any air mass set point into an intake pressure set point. For that purpose, let Ψ be a function which relates the aspirated air mass (denoted by m_{asp}) and the intake manifold pressure P_m in the form $m_{asp} \triangleq \Psi_{\Delta}(P_m, \delta\eta)$. In addition, m_{asp} can also be computed by integrating the mass air flow, $\dot{m}_{asp}$, over one period $\delta t = 120/N_e n_{cyl}$ (where n_{cyl} is the number of cylinders), i.e. $m_{asp} = \int_0^{\delta t} \dot{m}_{asp}\, dt$. Considering (7) as a steady-state relation, the function Ψ_{Δ} is defined by the averaging formula

$$m_{asp} = \Psi_{\Delta}(P_m, \delta\eta) \triangleq (\eta_{\Delta}(P_m) + \delta\eta)\beta_m P_m \delta t \tag{9}$$

3. Air path control

3.1. Motion planning: from m_{asp}^{sp} to P_m^{sp}

In vehicle applications, the driver prescribes a torque set point to the control system through the accelerator pedal. This information is directly transformed into an aspirated-air-mass set point m_{asp}^{sp}, using a look-up table which is experimentally determined on a test bench under steady-state conditions. This yields

$$m_{asp}^{sp} \triangleq \text{map}(T_q^{sp}, N_e)$$

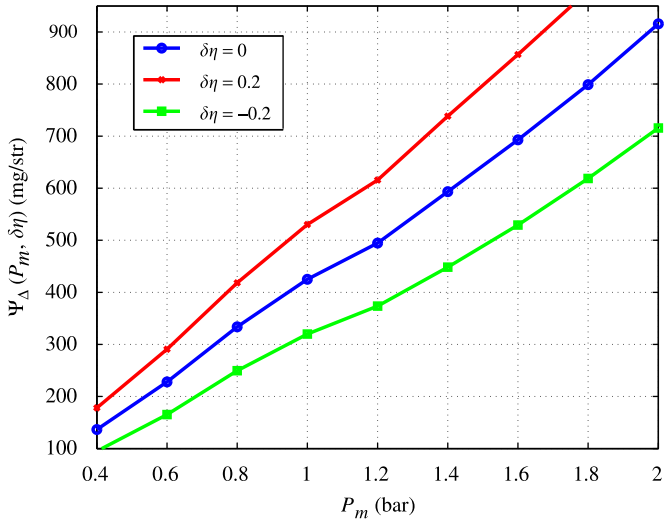

Fig. 5. One-to-one relation linking $\Psi_{\Delta}(P_m, \delta\eta)$ and P_m, at constant engine speed ($N_e = 2000$ rpm) and constant VVT actuator positions ($\Theta_{int} = 40^\circ$ and $\Theta_{int} = 0^\circ$).

A motion-planning-based method is proposed to reach this desired set point. Transients in the air path can be achieved by computing a feasible air mass trajectory. Inversion of the averaging formula (9) is trivial, since the function Ψ_{Δ} is bijective. Fig. 5 shows the one-to-one relation linking $\Psi_{\Delta}(P_m, \delta\eta)$ and P_m for different values of $\delta\eta$, at a given engine speed and given positions of the VVT actuators.

Inversion of the averaging formula (9) then yields

$$P_m^{sp} \triangleq \Psi_{\Delta}^{-1}(m_{asp}^{sp}, \delta\eta) = \Psi_{\Delta}^{-1}(\text{map}(T_q^{sp}, N_e), \delta\eta) \tag{10}$$

The air path has a first-order dynamics (8). Therefore, the in-cylinder air mass trajectory must be differentiable at least once. In practice, this minimal smoothness requirement is guaranteed by a low-pass filtering of the torque set point T_q^{sp}. Since Ψ_{Δ} is a continuous function, P_m^{sp} has the same continuity and differentiability properties as m_{asp}^{sp}. However, the bias $\delta\eta$ is unknown, and the trajectory P_m^{sp} cannot be explicitly computed. To compensate for this lack of information, an observer is needed to reconstruct $\delta\eta$ in order to be able to compute a pressure reference trajectory.

3.2. Air path observer: from P_m^{sp} to P_m^r

To compensate for this missing information, an observer (defined in (11)) is used to provide an estimate of x_2. A nonlinear observer based on pressure measurement can be considered in the form

$$\begin{cases} \dot{\hat{x}}_1 = \alpha_m(y_2 - (\eta_{\Delta}(y_1) + \hat{x}_2)\beta_m\hat{x}_1) + \alpha_m\beta_m l_1(y_1 - \hat{x}_1) \\ \dot{\hat{x}}_2 = -\alpha_m\beta_m\hat{x}_1 l_2(y_1 - \hat{x}_1) \end{cases} \tag{11}$$

where l_1 and l_2 are strictly positive constants. One may notice that (11) is a copy of (8) with additive tracking terms and injection of the output measurement y_2. The unknowns are partially substituted by output measurements. The convergence of this observer was proven by Leroy, Chauvin, and Petit (2008), leading to the following proposition.

Proposition 1. *The state of the observer* (11) *converges exponentially towards the state of the system* (8).

This observer gives a real-time estimation $\hat{\delta\eta}$ of $\delta\eta$ such that the error $\|\hat{\delta\eta} - \delta\eta\|$ converges exponentially towards 0. One can now

compute the reference pressure trajectory

$$P_m^r \triangleq \Psi_{\Delta}^{-1}(\mathrm{map}(T_q^{sp}, N_e), \hat{\delta\eta}) \tag{12}$$

Thus, as Ψ_{Δ} is continuous, Proposition 1 implies that

$\|P_m^r - P_m^{sp}\|$ converges exponentially towards 0.

3.3. Air path feedforward: from P_m^r to u^r

The system (8) is fully actuated and invertible. Provided that the bias ε_{th} is equal to zero and the bias $\delta\eta$ is known (or estimated), one can easily compute an open-loop control law for any smooth trajectory. This is, in theory, sufficient to guarantee tracking, owing to the open-loop stability of (8). Consider the following open-loop control law:

$$u^r = \mathscr{A}^{-1}\left(\frac{1}{f(x_1)}\left(\frac{\dot{x}_1^r}{\alpha_m} + (\eta_{\Delta}(x_1^r) + \hat{x}_2)\beta_m x_1^r\right)\right) \tag{13}$$

Tracking of the trajectory using the control law (13) was proven by Leroy, Chauvin, and Petit (2008) and leads to the following proposition.

Proposition 2. *Consider a perfect system* (8) *with* $\varepsilon_{th} = 0$ *and some smooth reference trajectory* x_1^r. *The open-loop control law* (13) (*which uses an estimated value of* x_2) *guarantees that the tracking error e converges exponentially towards* 0 *when* $t \to \infty$.

3.4. Air path control: from u^r to u^{sp}

In a more realistic setup, assume that the bias ε_{th} is not equal to zero. To compensate for this missing information, one adds an integral term to the feedback law, aimed at tracking the reference trajectory x_1^r. This leads us to consider the following control law:

$$u^{sp} = \mathscr{A}^{-1}\left(\mathscr{A}(u^r) - \frac{1}{\alpha_m f(x_1)}\left(k_p(x_1 - x_1^r) + k_i\int_0^t (x_1 - x_1^r)\,\mathrm{d}t\right)\right) \tag{14}$$

where k_p and k_i are strictly positive constants. Tracking of the trajectory using the control law (14) was proven by Leroy, Chauvin, and Petit (2008) and leads to the following proposition.

Proposition 3. *Consider the system* (8) *and some smooth reference trajectory* x_1^r. *The closed-loop control law guarantees that the tracking error converges asymptotically towards* 0 *when* $t \to \infty$.

3.5. Air path control

The air path control consists of an open-loop intake manifold pressure controller (see Section 3.3), a closed-loop controller (see Section 3.4), and an in-cylinder air mass observer (see Section 3.2). From Propositions 1 and 3, the following theorem holds.

Theorem 1. *Consider the in-cylinder air mass observer* (11) *and the intake manifold pressure closed-loop control strategy* (14). *Then the in-cylinder air mass converges asymptotically towards its set point, i.e.* $\|m_{asp} - m_{asp}^{sp}\| \to 0$ *when* $t \to \infty$.

Remark 1. When the measurement $\dot{m}_{MAF}$ of the intake mass air flow is not available, the observer (11) can no longer be used. Consequently, the control strategy (14) remains valid, i.e. P_m still converges towards P_m^r, but the reference pressure P_m^r does not converge any more towards P_m^{sp}. This stresses the importance of a good open-loop model for the in-cylinder air mass.

4. Experimental results

4.1. Implementation

The global control scheme is summarized in Fig. 6. The control strategy is twofold: air path control and injection control.

The air path controller uses the motion-planning control strategy presented in Section 3. The observer (11) feeds the pressure trajectory computation block. The reference trajectory of the pressure P_m^r obtained is then used in a dynamic model inversion to determine the feedforward control law θ_{th}^r. Finally, the PI controller presented in Section 3.4 gives the throttle-opening set point θ_{th}^{sp}.

The injection controller uses a feedforward control law based on the in-cylinder air mass trajectory, m_{asp}^{sp}, and feedback information given by a PID controller based on the exhaust FAR measurement. To take the injection delay and the computation

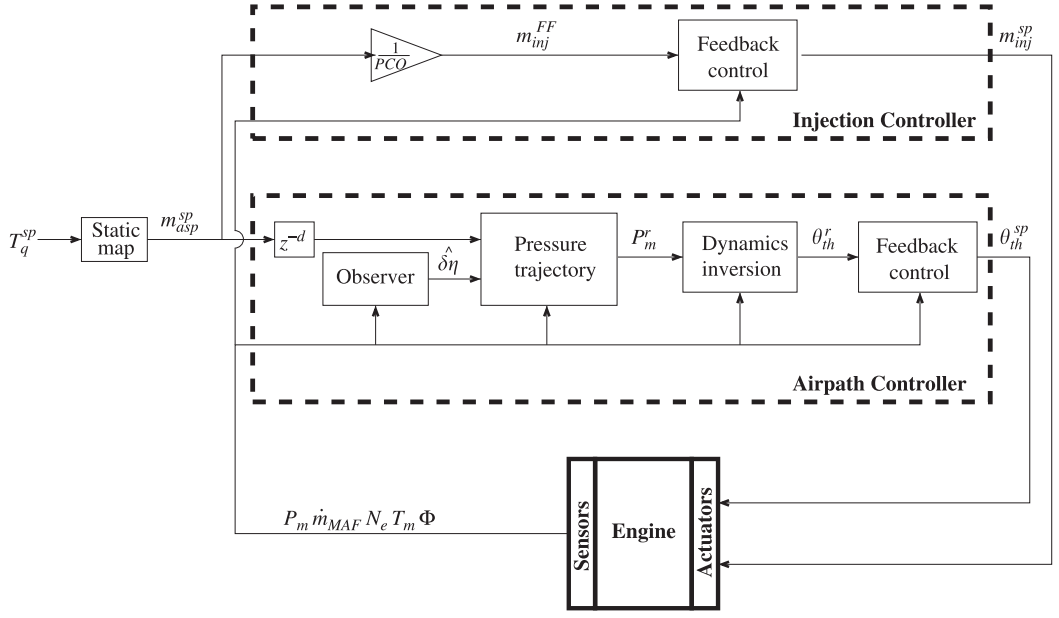

Fig. 6. Control scheme.

time into account (see Chevalier, Vigild et al., 2000), a delay is imposed on the air path control.

4.2. Engine setup

The engine under consideration was a 1.8 L four-cylinder SI engine using direct-injection technology and homogeneous combustion. The air path consisted of a turbocharger with a monoscroll turbine controlled by a wastegate, an intake throttle, and a downstream compressor heat exchanger permitting regulation of the intake air temperature. To take advantage of all of the versatility of direct injection and turbocharging, the engine was equipped with two VVT devices, for the intake and exhaust valves. This engine setup is consistent with the scheme reported in Fig. 2.

4.3. Experimental tip-in on test bench

The control strategy presented in this paper was tested on an experimental test bench. First, the response of the system to a fast torque tip-in is shown. Fig. 7 presents the transient behavior of the control strategy. Fig. 7a gives the in-cylinder air mass set point (directly derived from the torque set point though a look-up table; see Fig. 6) and the estimation of it given by the relation (9), using the observer (11) to estimate the bias $\delta\eta$. Fig. 7b presents the intake manifold reference trajectory, computed in (12), and its measurement. Finally, Fig. 7c shows the throttle position set point, given by the feedback control strategy (14), and its measurement.

These figures show good tracking of the trajectories of the intake manifold pressure and in-cylinder air mass. This tracking is possible thanks to fast throttle control. In fact, during a transient,

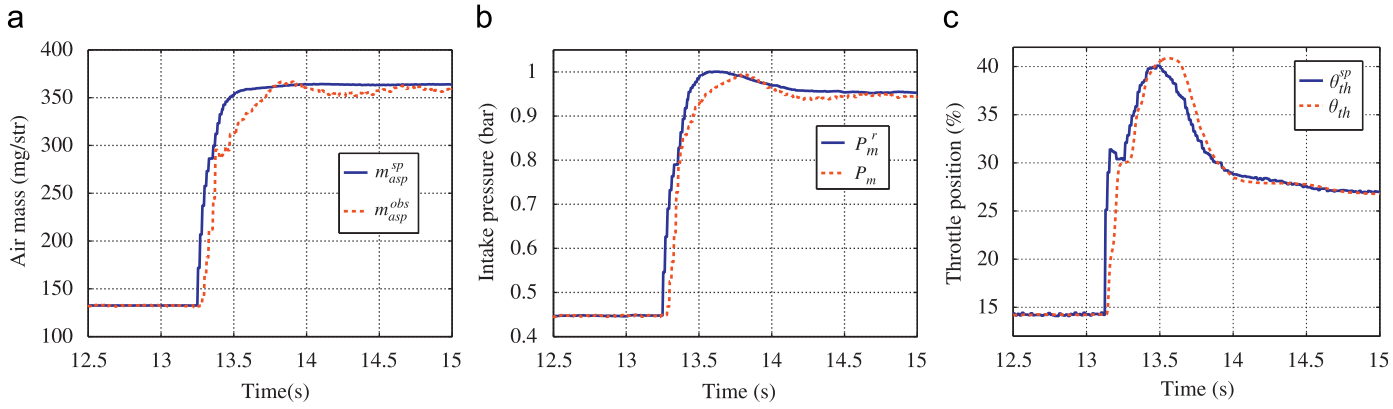

Fig. 7. Experimental results for a four-cylinder SI engine at constant engine speed (2000 rpm). Fast torque tip-in. (a) In-cylinder air mass; (b) intake manifold pressure; and (c) throttle position.

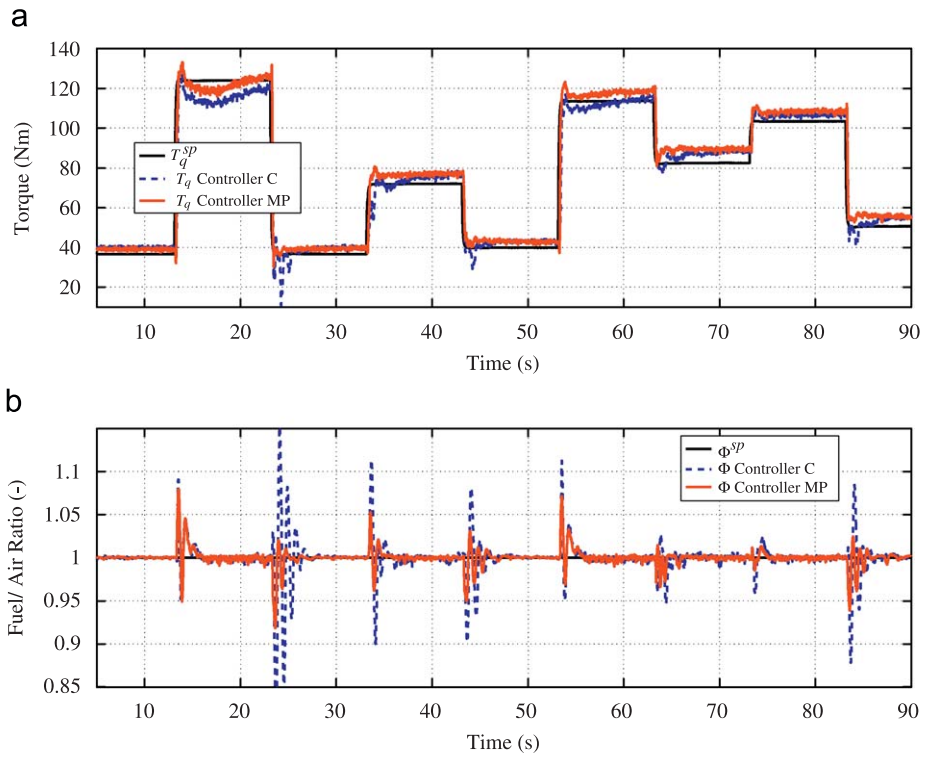

Fig. 8. Experimental results for a four-cylinder SI engine at constant engine speed (2000 rpm). Comparison of (a) torque and (b) fuel/air ratio control between two control strategies.

the feedforward term boosts the intake manifold pressure response thanks to the term $\dot{P}_m^r$ in the control strategy (14). One can see a peak in the throttle position set point at about 13.2 s.

4.4. Experimental transients on test bench: impact of the control strategy on torque and FAR control

Some torque transients were then applied to the engine in order to validate the proposed strategy and compare it with a classical strategy. One use the name 'Controller MP' to denote the strategy presented above, and 'Controller C' to denote the classical control strategy presented in Le Solliec, Le Berr, Colin, Corde, and Chamaillard (2007). This second strategy is based on a classical in-cylinder air mass prediction for FAR control and classical throttle position control (with a static feedforward term and feedback term).

Fig. 8 presents the results for the torque response (Fig. 8a) and FAR management (Fig. 8b). The torque response is better with the proposed control strategy. This improvement is twofold: (1) the motion-planning control strategy permits faster torque transients to be addressed, thanks to the throttle position control strategy (2), and (14) the FAR peaks are limited and thus affect the torque less. FAR management is also better with the proposed control strategy. Let $e \triangleq \phi^{sp} - \phi$ define the error between the stoichiometric FAR and the measured value, and consider the two

Table 1
Comparison of controller performance.

Performance metric	Controller C	Controller MP
$\|e\|_2$	2.8731	1.3932
$\|e\|_\infty$	0.1882	0.0814

Table 2
Comparison of controller performance over part of the NEDC driving cycle.

Performance metric	Controller C	Controller MP
$\|e\|_2$	21.8522	19.9365

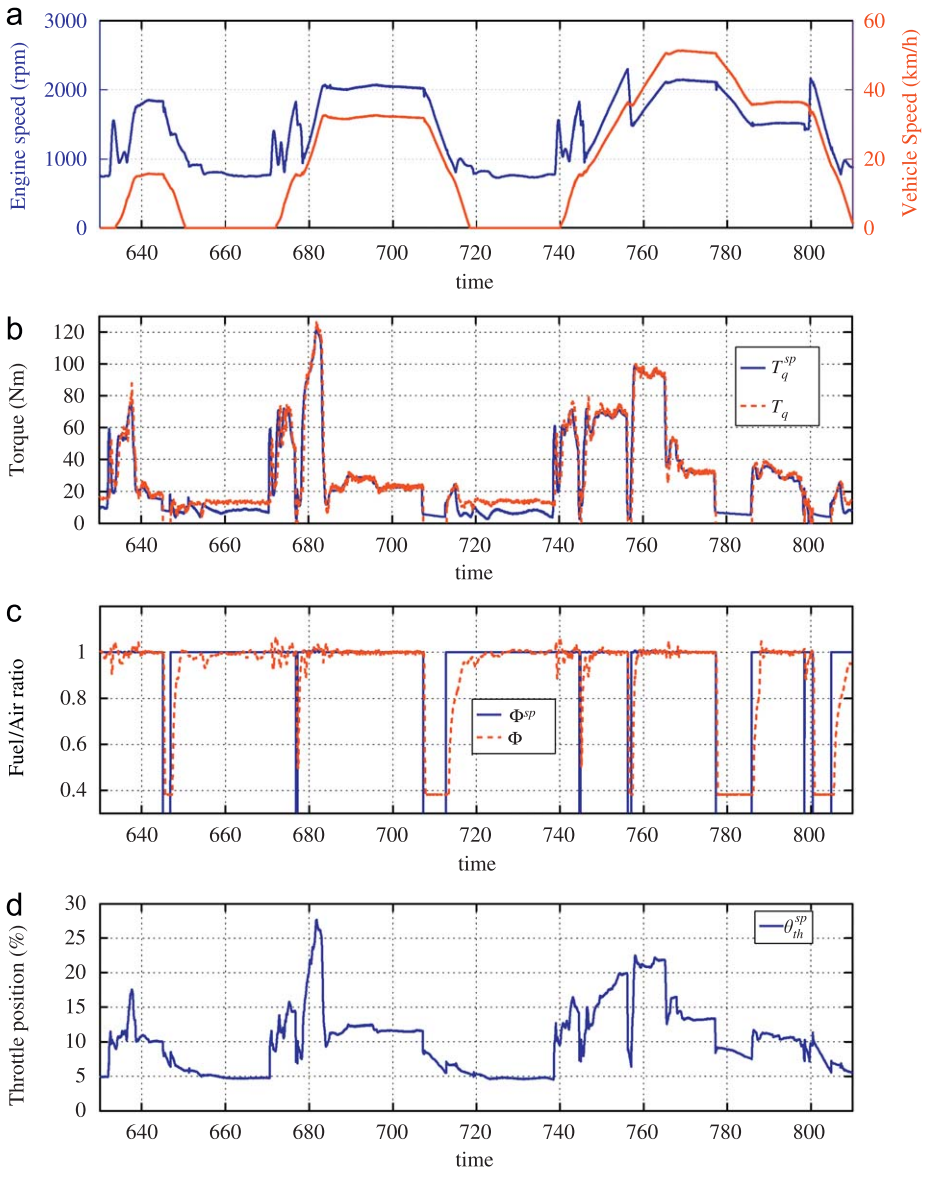

Fig. 9. Torque and FAR control results for vehicle during NEDC cycle. (a) Engine speed and vehicle speed; (b) torque; (c) fuel/air ratio; and (d) throttle position.

performance metrics $\|e\|_2$ and $\|e\|_\infty$. Table 1 compares the two controllers when used with the transients presented in Fig. 8.

4.5. Experimental results from an NEDC driving cycle

The proposed control strategy was integrated into a demonstration vehicle for experimental validation on a roller test bed. Fig. 9 gives some results obtained during a whole ECE cycle (part of the NEDC).

The vehicle speed and engine speed are represented in Fig. 9a. The vehicle speed and gear number were imposed on the driver. Fig. 9b presents the final results for torque control. Good tracking of the desired torque trajectory is provided thanks to the air path control strategy (the static errors come from biases in the look-up table). Fast transients are permitted, thanks to the motion-planning control strategy for the intake manifold pressure. The corresponding throttle position set point is given in Fig. 9d. Fig. 9c gives results for the FAR control using the strategy presented, i.e. the feedforward injected-fuel-mass control is directly derived from the in-cylinder trajectory. FAR excursions are limited; this means that good tracking of the in-cylinder air mass is achieved thanks to the control strategy. Table 2 compares the proposed controller with a classical controller during the whole ECE cycle. Owing to the presence of numerous, relatively long steady-state phases, the values of the criteria are close to each other, but remain in favor of the proposed methodology.

5. Conclusions

This paper presents a new approach for controlling the air path in an SI engine equipped with VVT actuators. The method is based on the tracking of a reference trajectory of the air mass in the cylinders. VVT actuators are considered as measured disturbances. A closed-loop control law based on measurement of the intake manifold pressure has been presented. The strategy has been tested on a test bench and improvements can be observed in FAR management (and thus, indirectly, in torque control) compared with a classical approach. This strategy has also been tested on a vehicle during the NEDC cycle.

The strategy has been experimentally validated under atmospheric conditions. The next step will be to consider turbocharging conditions. The strategy will remain the same, except that the air path dynamics is different under turbocharging conditions.

Notation

$\dot{m}_{asp}$	aspirated mass air flow (kg/s)
m_{asp}	in-cylinder air mass (kg)
$\dot{m}_{at}$	throttle mass air flow (kg/s)
N_e	number of crankshaft revolutions (rpm)
n_{cyl}	number of cylinders
P_{dc}	downstream compressor pressure (Pa)
P_m	intake manifold pressure (Pa)
R	ideal gas constant (J/kg K)
T_m	intake manifold temperature (K)
V_d	total displaced volume of all cylinders (m^3)
V_m	intake manifold volume (m^3)
$\delta\eta$	volumetric-efficiency bias
η_Δ	volumetric efficiency
Φ	fuel/air ratio
Θ_{exh}	exhaust valve timing actuator position°
Θ_{int}	intake valve timing actuator position°
θ_{th}	throttle opening angle

Acknowledgments

The authors are grateful to Gilles Corde and Guénaël Le Solliec for their scientific support.

References

Andersson, P. & Eriksson, L. (2001). Air-to-cylinder observer on a turbocharged SI-engine with wastegate. In *Proceedings of SAE conference*, no. 2001-01-0262.

Chevalier, A., Müller, M., & Hendricks, E. (2000). On the validity of mean value engine models during transient operation. In *Proceedings of SAE conference*, number 2000-01-1261.

Chevalier, A., Vigild, C., & Hendricks, E. (2000). Predicting the port air mass flow of SI engines in air/fuel ratio control applications. In *Proceedings of SAE conference*, no. 2000-01-0260.

Colin, G., Chamaillard, Y., Bloch, G., & Corde, G. (2007). Neural control of fast nonlinear systems—application to a turbocharged SI engine With VCT. *IEEE Transactions on Neural Networks*, *18*(4), 1101–1114.

Grizzle, J. W., Cook, J. A., & Milam, W. P. (1994). Improved cylinder air charge estimation for transient air fuel ratio control. In *Proceedings of the American control conference*.

Guzzella, L., & Onder, C. H. (2004). *Introduction to modeling and control of internal combustion engine systems*. Berlin: Springer.

Heywood, J. (1988). *Internal combustion engine fundamentals*. New York: McGraw-Hill.

Jankovic, M. (2002). Nonlinear control in automotive engine applications. In *Proceedings of 15th international symposium on mathematical theory of networks and systems*.

Jankovic, M., Frischmuth, F., Stefanopoulou, A., & Cook, J. A. (1998). Torque management of engines with variable cam timing. *Control Systems Magazine, IEEE*, *18*, 34–42.

Khiar, D., Lauber, J., Floquet, T., Colin, G., Guerra, T. M., & Chamaillard, Y. (2007). Torque management of engines with variable cam timing. *Control Engineering Practice*, *15*(12), 1446–1456.

Le Solliec, G., Le Berr, F., Colin, G., Corde, G., & Chamaillard, Y. (2007). Engine control of a downsized spark ignited engine: From simulation to vehicle. *Oil & Gas Science and Technology*, *62*, 555–572.

Lecointe, B., & Monnier G. (2003). Downsizing a gasoline engine using turbocharging with direct injection. In *Proceedings of SAE conference*, no. 2003-01-0542.

Leroy, T., Chauvin, J., Le Berr, F., Duparchy, A., & Alix, G. (2008). Modeling fresh air charge and residual gas fraction on a dual independent variable valve timing SI engine. In *Proceedings of SAE conference*, no. 2008-01-0983.

Leroy, T., Chauvin, J., & Petit, N. (2008). Airpath control of a SI engine with variable valve timing actuators. In *Proceedings of the American control conference*.

Shaver, G. M., Roelle, M. J., & Christian Gerdes, J. (2006). Modeling cycle-to-cycle dynamics and mode transition in HCCI engines with variable valve actuation. *Control Engineering Practice*, *14*(3), 213–222.

Stefanopoulou, A., Cook, J. A., Grizzle, J. W., & Freudenberg, J. S. (1998). Control-oriented model of a dual equal variable cam timing spark ignition engine. *ASME Journal of Dynamic Systems, Measurement Contributions*, *120*, 257–266.

Stefanopoulou, A., & Kolmanovsky, I. (1997). Dynamic scheduling of internal exhaust gas recirculation systems. *Proceedings of the IMECE*, *61*, 671–678.

Stefanopoulou, A., & Kolmanovsky, I. (1999). Analysis and control of transient torque response in engines with internal exhaust gas recirculation. *IEEE Transactions on Control Systems Technology*, *7*, 555–566.

Stotsky, A., & Kolmanovsky, I. (2002). Application of input estimation techniques to charge estimation and control in automotive engines. *Control Engineering Practice*, *10*, 1371–1383.